JOURNAL OF COMPUTATIONAL PHYSICS 48, 1–22 (1982)

A Numerical Study of the Two–Dimensional Navier–Stokes Equations in Vorticity–Velocity Variables

T. B. GATSKI

NASA Langley Research Center, Hampton, Virginia 23665

C. E. GROSCH*

Old Dominion University, Norfolk, Virginia 23508

AND

M. E. ROSE*

Institute for Computer Applications in Science and Engineering, NASA Langley Research Center, Hampton, Virginia 23665

Received November 24, 1981; revised March 31, 1982

Solution methods for compact finite-difference schemes are applied to the vorticity-velocity form of the two-dimensional unsteady Navier–Stokes equations. Numerical experiments for stagnation point and driven cavity flows are described.

1. INTRODUCTION

The flow of an incompressible viscous fluid in two dimensions is described in terms of the velocity $\mathbf{u} = (u, v)$ and vorticity ζ by the Navier–Stokes equations in the form

$$u_x + v_y = 0, \qquad v_x - u_y = \zeta, \tag{1.1a}$$

$$\zeta_t + \operatorname{div}(\mathbf{u}\zeta - \nu \operatorname{grad} \zeta) = 0, \tag{1.1b}$$

where ν is the kinematic viscosity. A direct finite-difference approach to the numerical solution of this system of equations serves to highlight inaccuracies which can arise from the treatment of boundary conditions when the normal and tangential components of the velocity are specified, particularly when a stream function is used to satisfy the continuity equation. Inaccuracies can also arise by the use of centered-

* Research was supported under NASA Contract No. NAS1-15810 at ICASE, NASA Langley Research Center, Hampton, Va. 23665. The third author was also supported under NASA Contract No. NAS1-16394.

0021-9991/82/100001-22$02.00/0

Copyright © 1982 by Academic Press, Inc.
All rights of reproduction in any form reserved.

difference expressions to treat transport terms when the local cell Reynolds number is large. The steady state solution of the driven cavity problem has provided a standard means of studying these numerical difficulties (cf. [2, 7, 9, 11]).

This paper contains the results of adapting a class of compact finite-difference schemes described by Rose [8] and Philips and Rose [6] to treat (1.1) directly in terms of the velocity **u** and the vorticity ζ. These schemes are second-order accurate in terms of the mesh parameters, the accuracy being independent of the local cell Reynolds number. Briefly described, the solution method is as follows: with an assumed distribution of vorticity, the velocity field is first determined so as to satisfy (1.1a) with prescribed values of the velocity normal to the boundary. A new distribution of vorticity is then determined by solving (1.1b) using boundary conditions for the vorticity which are implied by values of the tangential components of the velocity prescribed on the boundary. A repetition of the process then yields the velocity and vorticity at any later time. It appears that the only previous use of vorticity–velocity variables in numerical calculations is that of Fasel [4]. At each time step Fasel solves two Poisson equations for the components of **u**, derivable from the definition of vorticity.

Two numerical experiments are described. One treats the flow impinging on a flat plate, in which case we are able to compare the numerical results with the analytical steady state solution [1]. The other treats the driven cavity problem, our primary purpose being to describe the time evolution of this classical problem [3].

Section II describes the compact finite-difference equations whose solution yields an approximation to (1.1); the numerical schemes which provide the solution of these equations are discussed in Section III. The remaining sections report the results of applying these developments to the problems mentioned above.

II. Compact Difference Schemes for **u** and ζ

Consider the problem of approximating the solution of (1.1) in a rectangular domain D on whose boundary Γ both components of the velocity are prescribed. Subdivide the domain into rectangular computational cells $\pi^n_{jk}\{|x - x_j| < \Delta x/2, |y - y_k| < \Delta y/2, |t - t_n| < \Delta t/2\}$ and write $w^n_{jk} = w(j\Delta x, k\Delta y, n\Delta t)$. A typical cell and the location of the variables on that cell are shown in Fig. 1. A variable associated with the side of a cell is to be interpreted as the average of that variable over the side of the cell and one associated with the center of a cell is an average over the cell. We employ the notation

$$\mu_x w^n_{j,k} = (w^n_{j+1/2,k} + w^n_{j-1/2,k})/2, \qquad \delta_x w^n_{j,k} = (w^n_{j+1/2,k} - w^n_{j-1/2,k})/\Delta x, \ldots.$$

When no confusion is likely to arise we suppress the spatial indices and write $w^n_\cdot = w(\cdot, \cdot, n\Delta t)$; thus $\mu_x w^n_\cdot$, $\delta_x w^n_\cdot$, $\mu_y w^n_\cdot$, $\delta_y w^n_\cdot$, $\mu_t w^n_\cdot$, $\delta_t w^n_\cdot$ involve values associated with the faces of the cell $\pi^n_\cdot$. A finite-difference scheme which involves

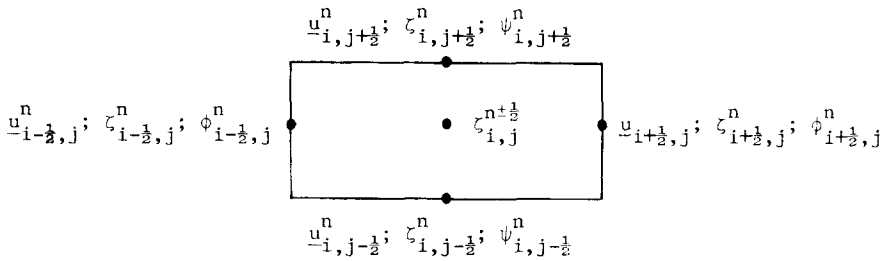

FIG. 1. Values associated with the sides of a computational cell.

only data associated with velocity equations (1.1a) and vorticity convective–diffusion equation (1.1b) are:

A. *Velocity Equations*

Suppose values $\zeta_{\cdot}^{n-1/2}$ are prescribed. Following [8], the velocity components at time $t = t_n$ are determined by the solution of the compact difference equations

$$\delta_x v_{\cdot}^n - \delta_y u_{\cdot}^n = \zeta_{\cdot}^{n-1/2}, \qquad \delta_x u_{\cdot}^n + \delta_y v_{\cdot}^n = 0, \tag{2.1a}$$

$$(\mu_x - \mu_y)\, u_{\cdot}^n = 0, \qquad (\mu_x - \mu_y)\, v_{\cdot}^n = 0, \tag{2.1b}$$

when, say, the components of the velocity normal to the boundary are prescribed.

B. *Vorticity Equations*

Write (1.1b) in system form as

$$\zeta_t + \operatorname{div}(\mathbf{u}\zeta) = \nu(\phi_x + \psi_y), \qquad \zeta_x = \phi, \qquad \zeta_y = \psi, \tag{2.2}$$

and suppose that the velocity field $\mathbf{u}_{\cdot}^n$ has been determined at time $t = t_n$. Following [6], a compact difference scheme for (2.2) is given by

$$(\delta_t + (\mu_x u_{\cdot}^n)\, \delta_x + (\mu_y v_{\cdot}^n)\, \delta_y)\, \zeta_{\cdot}^n = \nu(\delta_x \phi_{\cdot}^n + \delta_y \psi_{\cdot}^n), \tag{2.3a}$$

$$\mu_t \zeta_{\cdot}^n = \mu_x \zeta_{\cdot}^n = \mu_y \zeta_{\cdot}^n, \tag{2.3b}$$

$$\delta_x \zeta_{\cdot}^n = (\mu_x - \tfrac{1}{2}\, \Delta x\, q(\theta_x)\, \delta_x)\, \phi_{\cdot}^n, \tag{2.3c}$$

$$\delta_y \zeta_{\cdot}^n = (\mu_y - \tfrac{1}{2}\, \Delta y\, q(\theta_y)\, \delta_y)\, \psi_{\cdot}^n, \tag{2.3d}$$

in which

$$\theta_x = u\, \Delta x/2\nu, \qquad \theta_y = v\, \Delta y/2\nu, \tag{2.4}$$

and

$$q(\theta) = \coth \theta - \theta^{-1}. \tag{2.5}$$

As described below, the solution of (2.3) yields $\zeta_{\cdot}^{n+1/2}$ in terms of $\zeta_{\cdot}^{n-1/2}$ and boundary conditions for $\zeta_{\cdot}^{n}$. We shall employ the approximations

$$\begin{aligned} q(\theta) &\simeq \theta/3, && \text{for} \quad \theta \text{ small}, \\ &\simeq \operatorname{sgn}\theta - \theta^{-1}, && \text{for} \quad \theta \text{ large}, \end{aligned} \tag{2.6}$$

where $\operatorname{sgn}\theta = \theta/|\theta|$.

In order to understand the role of the function $q(\theta)$ in (2.3) consider the differential equation $u_t + au_x - vu_{xx} = 0$, where $a = \text{const}$. This equation has exponential solutions of the form $\phi(x, t; \alpha) = \exp(\alpha x - \beta(\alpha)\, t)$, where $\beta(\alpha) = \alpha(a - v\alpha)$. For $\alpha = 0$ or $\alpha = a/v$, $\beta = 0$ and a steady-state solution results. Consider the family of solutions

$$u = c_1\phi(x, t; 0) + c_2\left(\frac{\partial}{\partial\alpha}\phi(x, t; \alpha)\right)_{\alpha=0} + c_3\phi(x, t; a/v),$$

where c_1, c_2, c_3 are parameters, viz., $u = c_1 + c_2(x - at) + c_3\exp(ax/v)$. The difference operator

$$L_\xi = \begin{pmatrix} \delta_t + a\delta_x & -v\delta_x \\ \delta_x & -(\mu_x - q\xi\,\delta_x) \end{pmatrix},$$

where $\xi = \Delta x/2$, results in a truncation error $(\varepsilon_1(\alpha), \varepsilon_2(\alpha))^{\mathrm{T}}\,\phi(x, t; \alpha)$ given by

$$L_\xi \begin{pmatrix} 1 \\ \alpha \end{pmatrix} \phi(x, t; \alpha) = \begin{pmatrix} \varepsilon_1(\alpha) \\ \varepsilon_2(\alpha) \end{pmatrix} \phi(x, t; \alpha),$$

where, if $\tau = \Delta t/2$,

$$\begin{aligned} \varepsilon_1(\alpha) &= -\tau^{-1}\sinh\beta(\alpha)\,\tau + (a - v\alpha)\,\xi^{-1}\sinh\alpha\xi, \\ \varepsilon_2(\alpha) &= (\xi^{-1} + q\alpha)\sinh\alpha\xi - \alpha\cosh\alpha\xi. \end{aligned}$$

Hence $\varepsilon_1(0) = \varepsilon_2(0) = 0$ and also $\partial\varepsilon_2/\partial\alpha\,|_{\alpha=0} = \partial\varepsilon_2/\partial\alpha\,|_{\alpha=0} = 0$ so that the truncation error arising from the basis $\phi(x, t; 0)$, $\phi_\alpha(x, t; 0)$ vanishes. For $\alpha = a/v$ the truncation error is, since $\beta(a/v) = 0$,

$$\varepsilon_1(a/v) = 0, \qquad \varepsilon_2(a/v) = \alpha\sinh\alpha\xi((\alpha\xi)^{-1} + q - \coth\alpha\xi)\,|_{\alpha=a/v}$$

so that $\varepsilon_2(a/v) = 0$ when $q(a\xi/v)$ is given by (2.5). Thus the parameter $q(\theta)$ serves to reduce the truncation error of the difference scheme to zero on the linear solution space spanned by $\phi(x, t; 0)$, $\phi_\alpha(x, t; 0)$ and $\phi(x, t; a/v)$ independently of the value of the local cell Reynolds parameter $\theta = a\,\Delta x/2v$.

As discussed in [6], (2.3) can be expected to provide a convergent approximation to (2.2) for any fixed values of $\lambda_x = \Delta t/\Delta x$ and $\lambda_y = \Delta t/\Delta y$ when $\Delta t \to 0$ which is second-order accurate independent of the values of the cell Reynolds numbers $|\theta_x|$ and $|\theta_y|$.

III. Numerical Solution of the Velocity and Vorticity Difference Equations

Because of their compact form, velocity and vorticity difference equations (2.1) and (2.3) present novel challenges for their numerical solution. While the approaches to be described in this section appear to offer effective solution procedures, they lack an efficiency which would be desirable for extended applications. We hope to report on progress toward the goal of developing more efficient techniques in a later paper.

A. *Velocity Equations*

We are indebted to Brandt and Nicolaides for bringing to our attention an iteration scheme due to Kaczmarz [5] which provides an effective means for treating the velocity equations (2.1).

Kaczmarz's scheme is most simply described for the general system of algebraic equations $Ax = b$ in which A is $n \times n$ (Tanabe [10] has discussed the extension to general $m \times n$ systems). Let A_j denote the jth row of A and let $R(x) = Ax - b$; if $r_j(x)$ denotes the jth component of $R(x)$ and if $x^{(k)}$ indicates the approximation to x at the kth iteration, then the scheme is described by

$$x^{(k+1)} = x^{(k)} + \omega A_j^{\mathrm{T}}(A_j A_j^{\mathrm{T}})^{-1} \cdot r_j(x^{(k)}), \qquad j = 1, 2, \ldots, n, \quad k = j \pmod{n}. \tag{3.1}$$

Here ω is an extrapolation parameter. Since the scheme is a projection method, (3.1) describes an SOR-type iterative technique.

In a personal communication, Nicolaides has shown that (3.1) may be applied when it is partitioned so that A_j is $l \times n$. Let

$$U = (u, v)^{\mathrm{T}}, \qquad \vec{\zeta} = (0, \zeta)^{\mathrm{T}}, \qquad \text{and} \qquad C = \begin{pmatrix} 0 & 1 \\ -1 & 0 \end{pmatrix};$$

also, define residuals $R_1(U_{\cdot}^{(k)})$, $R_2(U_{\cdot}^{(k)})$ by

$$R_1(U_{\cdot}^{(k)}) \equiv \delta_x U_{\cdot}^{(k)} + C\,\delta_y U_{\cdot}^{(k)} - \vec{\zeta}_{\cdot}^{(k)}, \qquad R_2(U_{\cdot}^{(k)}) \equiv \mu_x U_{\cdot}^{(k)} - \mu_y U_{\cdot}^{(k)}. \tag{3.2}$$

Then iteration scheme (3.1) applied to velocity equations (2.1) for the values of U associated with the sides of a computational cell leads to

$$U_{\cdot}^{(k+1)} = U_{\cdot}^{(k)} + \omega B^{\mathrm{T}}(B \cdot B^{\mathrm{T}})^{-1} \begin{pmatrix} R_1(U_{\cdot}^{(k)}) \\ R_2(U_{\cdot}^{(k)}) \end{pmatrix}, \tag{3.3}$$

where

$$B \equiv \begin{pmatrix} \lambda I, & -\lambda I, & C & -C \\ I, & I, & -I, & -I \end{pmatrix}, \tag{3.4}$$

in which I is the 2×2 identity matrix and $\lambda = \Delta y/\Delta x$. In numerical experiments reported below, experimentally determined values of ω were employed.

At cells which are incident to the boundary of the fundamental computational domain, certain components of U will be specified by boundary conditions. This will require a slight modification of the matrix B, the details of which will not be described here.

B. *Vorticity Boundary Conditions*

In the applications considered in this paper, iteration scheme (3.3) was used to solve velocity equations (2.1) when the normal component of the velocity field was prescribed on the boundary Γ of the computational domain. The result yields a velocity field $\mathbf{u}^n$ at time $t = t_n$ which, generally, violates the additional boundary condition for the tangential component of the velocity also specified on Γ. The vorticity ζ^n resulting from this computed velocity field may be calculated from the definition $\zeta^n = v_x^n - u_y^n$ using second-order accurate approximations to the derivatives u_y^n, v_x^n based upon calculated values of the velocity field interior to the computational domain. One may also calculate the vorticity $\bar{\zeta}^n$ which would result were the prescribed tangential velocity employed instead. The difference $\bar{\zeta}^n - \zeta^n$ will approximately represent the increment of vorticity needed to satisfy the additional tangential velocity condition arising from velocity equations (2.1). The vorticity $\bar{\zeta}^n$ will provide the boundary values required for the solution of (2.3) in a manner now to be described.

Figure 2 illustrates the situation at a point P_0 at the right-hand boundary in which P_{-1}, P_{-2} are the immediate interior neighbors of P_0 which lie along the extended interior normal to the boundary Γ.

If, at P_0, the normal component u of the velocity has been prescribed, say $u = \bar{u}$, then $\bar{u}_y$ will also determine u_y at P_0. The vorticity associated with the solution of velocity equations (2.1) which results from prescribing this normal boundary condition at P_0 is

$$\zeta^n(P_0) = (3v^n(P_0) - 4v^n(P_{-1}) + v^n(P_{-2}))/2\,\Delta x - \bar{u}_y(P_0), \tag{3.5}$$

which expresses the condition $\zeta = v_x - u_y$ at P_0. The vorticity $\bar{\zeta}^n(P_0)$ which results by imposing instead the prescribed tangential velocity, say $v(P_0) = \bar{v}(P_0)$, is then

$$\bar{\zeta}^n(P_0) = (3\bar{v}(P_0) - 4v^n(P_{-1}) + v^n(P_{-2}))/2\,\Delta x - \bar{u}_y(P_0).$$

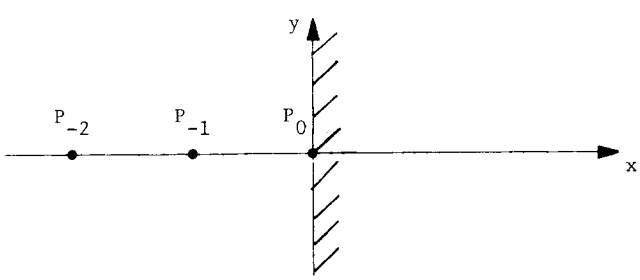

FIG. 2. Interior neighbors of a boundary point.

Similar expressions enable vorticity values $\bar{\zeta}^n$ to be calculated on the entire boundary Γ of the computational domain and will serve to provide boundary conditions required for the solution of vorticity equations (2.3) as next described.

C. *Vorticity Equations*

With a velocity field $\mathbf{u}^n$ determined as in III(A) and vorticity boundary data $\bar{\zeta}^n$ determined as in III(B) the vorticity $\zeta^{n+1/2}$at $t = t_{n+1/2}$ may be determined by a solution algorithm described by Philips and Rose [6]. Briefly stated, the procedure is as follows: with $\tau = \Delta t/2$ let

$$
\begin{aligned}
P_x &\equiv \begin{pmatrix} \mu_x + \tau(\mu_x u^n_{\cdot}) \, \delta_x, & -\nu\tau\delta_x \\ \delta_x, & \tfrac{1}{2}\,\Delta x \, q(\theta_x)\,\delta_x - \mu_x \end{pmatrix}, \\
P_y &\equiv \begin{pmatrix} \mu_y + \tau(\mu_y v^n_{\cdot}) \, \delta_y, & -\nu\tau\delta_y \\ \delta_y, & \tfrac{1}{2}\,\Delta y \, q(\theta_y)\,\delta_y - \mu_y \end{pmatrix}, \\
Q_x &\equiv \begin{pmatrix} (\mu_x u^n_{\cdot})\,\delta_x, & -\nu\delta_x \\ 0, & 0 \end{pmatrix}, \\
Q_y &\equiv \begin{pmatrix} (\mu_y v^n_{\cdot})\,\delta_y, & -\nu\delta_y \\ 0, & 0 \end{pmatrix}.
\end{aligned}
\tag{3.6}
$$

By eliminating the values $\zeta^{n+1/2}$ occurring in (2.3a) and (2.3b) the result is

$$
P_x \begin{pmatrix} \zeta^n_{\cdot} \\ \phi^n_{\cdot} \end{pmatrix} + \tau Q_y \begin{pmatrix} \zeta^n_{\cdot} \\ \psi^n_{\cdot} \end{pmatrix} = \begin{pmatrix} \zeta^{n-1/2}_{\cdot} \\ 0 \end{pmatrix}, \qquad P_y \begin{pmatrix} \zeta^n_{\cdot} \\ \psi^n_{\cdot} \end{pmatrix} + \tau Q_x \begin{pmatrix} \zeta^n_{\cdot} \\ \phi^n_{\cdot} \end{pmatrix} = \begin{pmatrix} \zeta^{n-1/2}_{\cdot} \\ 0 \end{pmatrix}. \tag{3.7}
$$

A two step procedure to determine $\zeta^{n+1/2}$ is

Step 1. Solve (3.7) for $(\zeta^n_{\cdot}, \phi^n_{\cdot}, \psi^n_{\cdot})$ using the ADI approximation

$$
\begin{pmatrix} \zeta^n_{\cdot} \\ \phi^n_{\cdot} \end{pmatrix} = P_x^{-1}(I - \tau Q_y P_y^{-1}) \begin{pmatrix} \zeta^{n-1/2}_{\cdot} \\ 0 \end{pmatrix}, \qquad \begin{pmatrix} \zeta^n_{\cdot} \\ \psi^n_{\cdot} \end{pmatrix} = P_y^{-1}(I - \tau Q_x P_x^{-1}) \begin{pmatrix} \zeta^{n-1/2}_{\cdot} \\ 0 \end{pmatrix}, \tag{3.8}
$$

in which the solution operators P_x^{-1} and P_y^{-1} may be constructed by an algebraic method described in [6] using boundary values for the vorticity $\bar{\zeta}^n$ developed in III(B). The accuracy of the approximation of (3.8) to (3.7) is $O(\tau^2)$.

Step 2. With the solution of (3.7) determined by Step 1, $\zeta^{n+1/2}_{\cdot}$ may be obtained using either leapfrog equation (2.3a) or, more simply, Eq. (2.3b).

The solution operator P_x^{-1} or P_y^{-1} arising in (3.8) may be determined more directly as follows: consider

$$
P_x \begin{pmatrix} \zeta^n_{\cdot} \\ \phi^n_{\cdot} \end{pmatrix} = \begin{pmatrix} g^n_{\cdot} \\ 0 \end{pmatrix}. \tag{3.9}
$$

Recalling definition (2.5), write $\hat{u}^n_{\cdot} = (\mu_x u^n_{\cdot})$, $q_x = q(\theta_x)$, $\lambda_x = \Delta t/\Delta x$, $\kappa_x = 2\nu\,\Delta t/\Delta x^2$. As shown in [6] the solution $\zeta^n_{\cdot}$ of (3.9) is determined as the solution of the tridiagonal system

$$\begin{aligned} &\tfrac{1}{2}[(1-q_x)(1+\lambda_x\hat{u}^n_{\cdot}) - \kappa_x]\,\zeta^n_{k+1} + \tfrac{1}{2}[(1+q_x)(1-\lambda_x\hat{u}^n_{\cdot}) - \kappa_x]\,\zeta^n_{k-1} \\ &\quad + [1 + \lambda\hat{u}^n_{\cdot}q_x + \kappa_x]\,\zeta^n_k = (1-q_x)\,g^n_{k+1/2} + (1+q_x)\,g^n_{k-1/2} \end{aligned} \tag{3.10}$$

for $k = 0, 1, \ldots, M-1$, where ζ_0 and ζ_M are given by the boundary data determined by $\bar{\zeta}$ as described in III(B). The solution of (3.10) then determines $\phi^n_{\cdot}$ as

$$\begin{aligned} \nu\lambda_x\phi^n_{k+1} &= \tfrac{1}{2}[(1+q_x)(1+\lambda_x\hat{u}^n_{\cdot}) + \kappa_x]\,\zeta^n_{k+1} + \tfrac{1}{2}[(1+q_x)(1-\lambda_x\hat{u}^n_{\cdot}) - \kappa_x]\,\zeta^n_k \\ &\quad - (1+q_x)\,g^n_{k+1/2}, \\ \nu\lambda_x\phi^n_k &= \tfrac{1}{2}[(q_x-1)(1+\lambda_x\hat{u}^n_{\cdot}) + \kappa_x]\,\zeta^n_{k+1} + \tfrac{1}{2}[(q_x-1)(1-\lambda_x\hat{u}^n_{\cdot}) - \kappa_x]\,\zeta^n_k \\ &\quad + (1-q_x)\,g^n_{k+1/2}. \end{aligned} \tag{3.11}$$

An analogous solution procedure for P_y^{-1} yields $(\zeta^n_{\cdot}, \psi^n_{\cdot})$. Thus, ADI scheme (3.8) can be implemented by repeated solution of equations of the type described by (3.10) and (3.11).

As is eveident from (2.6), when θ_x is large, then $q_x \simeq \operatorname{sgn}\theta_x$. In that case (3.10) is approximately a bidiagonal difference equation so that one of the two prescribed boundary conditions has little influence upon the solution, i.e., the difference scheme automatically incorporates a downwind or upwind differencing bias.

Finally, as indicated above, although difference scheme (2.3) is unconditionally stable, it is only second-order accurate; the approximation (3.8) was chosen to yield a similar accuracy. This, together with the SOR type of convergence resulting from the use of the Kaczmarz iteration scheme described in III(A), indicates a need to explore more efficient solution procedures for compact difference schemes of the type considered here for steady state problems.

IV. Stagnation Point Flow

A useful problem for testing the method concerns a steady flow impinging on a solid boundary. In the following, the x axis coincides with the boundary, the y axis is normal to the boundary, and the origin is a stagnation point of the flow. An exact steady-state solution of (1.1) is given as follows (cf. [1]):

If U_0 and l are the velocity and length scales of this flow, the stream function is

$$\psi = (U_0 l/\sqrt{\mathrm{Re}})\,\xi f(\eta), \tag{4.1}$$

where $\xi = x/l$, $\eta = \sqrt{\mathrm{Re}}\,(y/l)$, Re is the Reynolds number $\mathrm{Re} = U_0 l/\nu$, and $f(\eta)$ is the solution of

$$f''' + ff'' - (f')^2 + 1 = 0, \qquad f(0) = f'(0) = 0, \qquad f'(\infty) = 1.$$

The velocity components and the vorticity are then

$$u = U_0 \xi f'(\eta), \qquad v = -(U_0/\sqrt{\mathrm{Re}}) f(\eta), \qquad \zeta = -(U_0 \sqrt{\mathrm{Re}}/l)\, \xi f''(\eta). \quad (4.2)$$

If μ is the dynamic viscosity, the shear stress at the wall is then given by

$$\tau_0 = \mu u_y \,|_{y=0} = -\mu \zeta(x, 0). \quad (4.3)$$

The test problem is formulated as follows: the computational domain is

$$0 \leqslant x \leqslant l/2; \qquad 0 \leqslant y \leqslant l/2,$$

the choice of l being a matter of convenience. Formulae (4.2) for u and v, when averaged over the side of a computational cell, yield values employed for the normal and tangential velocity boundary conditions.

This problem is intended to test the accuracy of the numerical method independently of any errors introduced by approximate numerical boundary conditions, particularly outflow boundary conditions. For this reason, we used (4.2) to determine the exact normal velocity component and used this as the boundary condition for the velocity calculation. We hope to report the results of experiments with other boundary conditions in a subsequent paper.

Starting with initial data for u, v, and ζ in the interior, difference equations (1.1) were solved by the method described in Section III. A steady state was assumed to result when L_2 norms for the energy, vorticity, and enstrophy (squared vorticity) were constant in time within 0.01 percent. The reported errors Δu, Δv, and $\Delta\zeta$ in the values u, v, and ζ represent the difference between the computed values of u, v, and ζ as obtained from (2.1) and (2.3) and values obtained by the exact formulae (4.2) when averaged over sides of a computational cell. We have used two L_2 error norms to estimate the accuracy of our results: $\|\Delta u\|$ is the L_2 norm of Δu summed over the entire computational domain and normalized by the maximum value of $|\mathbf{u}|$ in the domain, while $\|\Delta\zeta\|_B$ is the L_2 norm of ζ on the solid wall boundary $y = 0$, also normalized by the maximum value of $|\zeta|$. In view of (4.3), $\|\Delta\zeta\|_B$ is also a measure of the error of the wall shear stress.

Table I contains the results of tests in which the number of cells in the computational domain was increased from 8×8 to 64×64 when $\mathrm{Re} = 100$. The L_2 norm $\|\Delta u\|$ is tabulated as a function of the number of cells as are the successive ratios of these values as the mesh ratio is doubled. The results given in Table I confirm the second-order accuracy of the scheme.

A second series of experiments was conducted to study the effect of increasing the Reynolds number when other parameters were held fixed. Defining the boundary layer thickness δ as the distance from the boundary at which the ratio of the velocity to its free stream value is 0.99 it can be shown that, for this flow,

$$\delta = 2.38 l/\sqrt{\mathrm{Re}}.$$

For a fixed mesh the result of increasing the Reynolds number is, then, to decrease

TABLE I

L_2 Error Norms for Stagnation Point Flow When Re = 100 as a Function of the Number of Cells in the Computational Domain

Number of cells	$\|\Delta u\|$	Ratio
8×8	3.00×10^{-3}	—
16×16	8.72×10^{-4}	3.44
32×32	2.40×10^{-4}	3.63
64×64	6.16×10^{-5}	3.90

Note. The ratio is that of the error norm for the next coarsest mesh to that of the error norm on the mesh.

the number of computational cells lying within the boundary layer. The results are presented in Figs. 3 and 4, where $\|\Delta u\|$ and $\|\Delta\zeta\|_B$ are plotted in terms of the Reynolds number; the horizontal scale $(\delta/\Delta y)$ is the number of cells within the boundary layer. An examination of these results shows that if $\mathrm{Re} < 10^3$, in which case five or more cells lie within the boundary layer, then $\|\Delta u\| < 0.1\%$ and $\|\Delta\zeta\|_B < 1\%$, while if at least 2 cells lie within the boundary layer, then $\|\Delta u\| < 1\%$ and $\|\Delta\zeta\|_B < 10\%$. Thus, engineering accuracy can be expected when, say, two or more cells lie within the boundary layer.

For $\mathrm{Re} \to \infty$, the problem under discussion results in a well-known potential flow. The inability of our scheme to capture this asymptotic result when the mesh is held

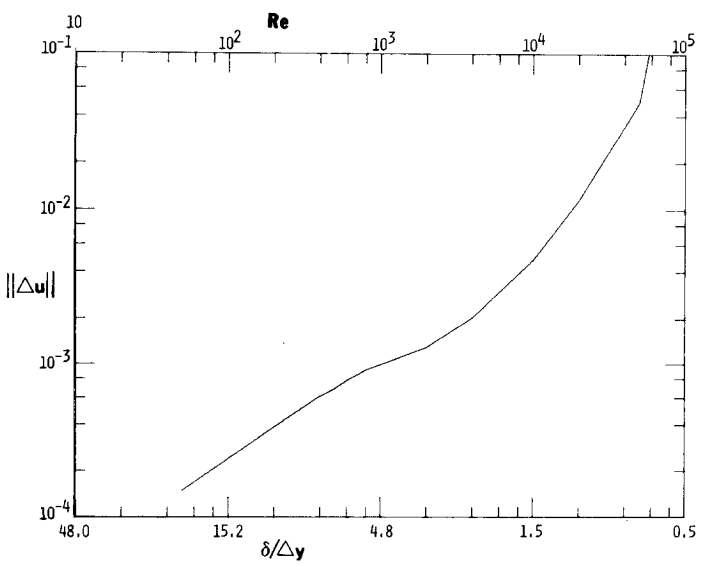

FIG. 3. Velocity error norm versus number of cells in boundary layer $(\delta/\Delta y)$.

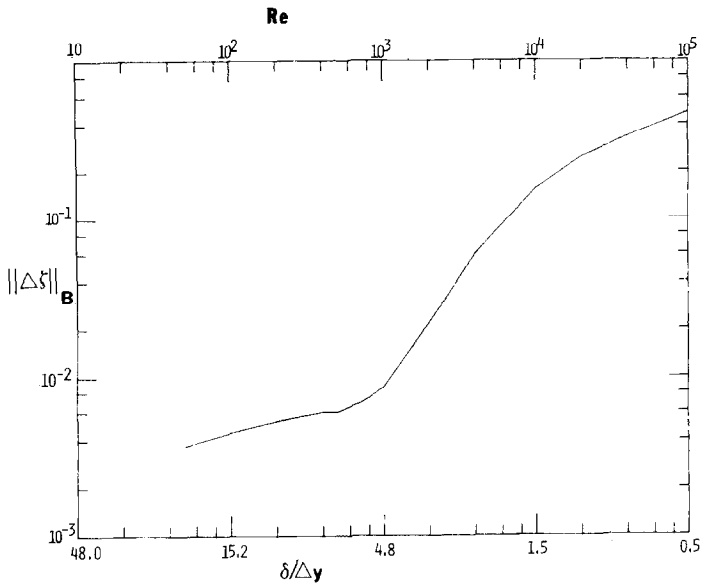

FIG. 4. Vorticity error norm versus number of cells in boundary layer ($\delta/\Delta y$).

fixed and $\mathrm{Re} \to \infty$ is shown in Figs. 3 and 4. This is primarily due to inaccuracies resulting from the use of (3.5) to estimate the vorticity generated at the boundaries.

V. THE DRIVEN CAVITY

As noted in the Introduction, the steady-state driven cavity has been studied extensively in terms of a stream function (among references we mention [2, 9]). This section describes features of the time-dependent solution $(\mathbf{u}, \zeta)$ obtained by solving (2.1) and (2.3) (cf. [3]).

The time evolution of the velocity and vorticity of an incompressible fluid initially at rest in a square cavity whose top wall of length l moves impulsively to the right with velocity U_0 are shown in Figs. 5 and 6. The results for the Reynolds number $\mathrm{Re} = lU_0/\nu$ are shown for $\mathrm{Re} = 400$. The computation employed 32×32 square cells and the value $\Delta t = 0.03125$ was used in (2.3).

As shown in Figs. 5a–d, the boundary layer at the moving wall is fully developed by the time $t = 1$ and is followed by a vortex which gradually moves toward the center of the cavity; a recirculation region is developed when an approximate steady state is reached at time $t = 22$. The main features of this development are also illustrated by the vorticity contours shown in Figs. 6a–d, in which the dashed lines represent negative vorticity and the solid lines represent positive vorticity.

the initial formation of the boundary layer at the moving wall ($t = 1$) little change in

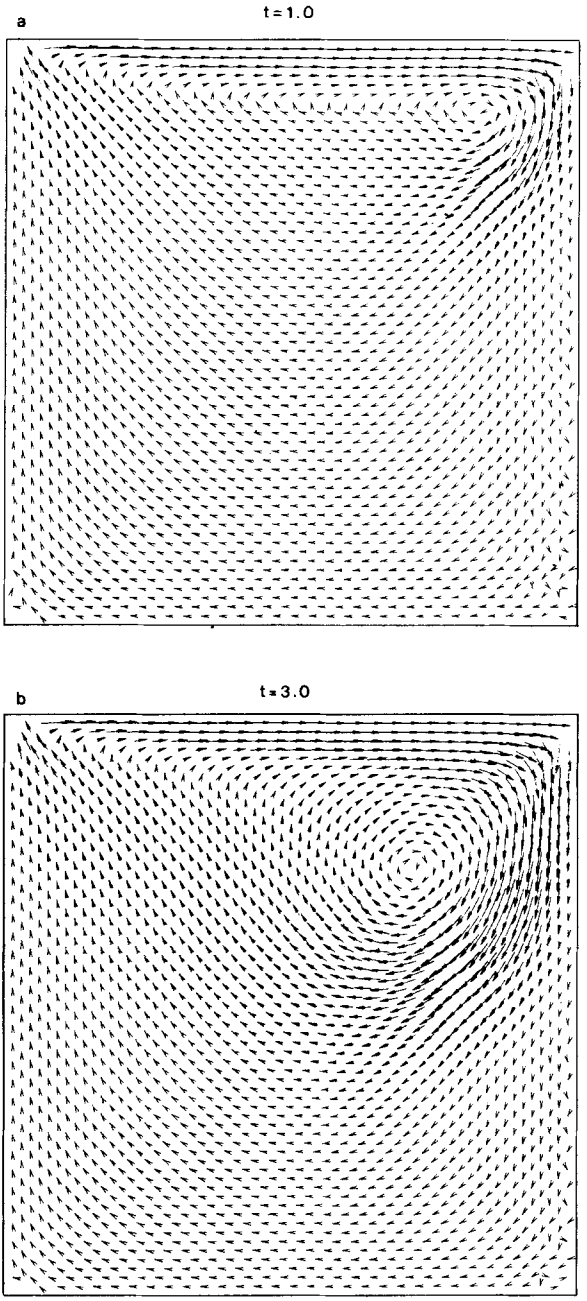

FIG. 5. Evolution of velocity field to steady state in a square cavity (Re = 400).

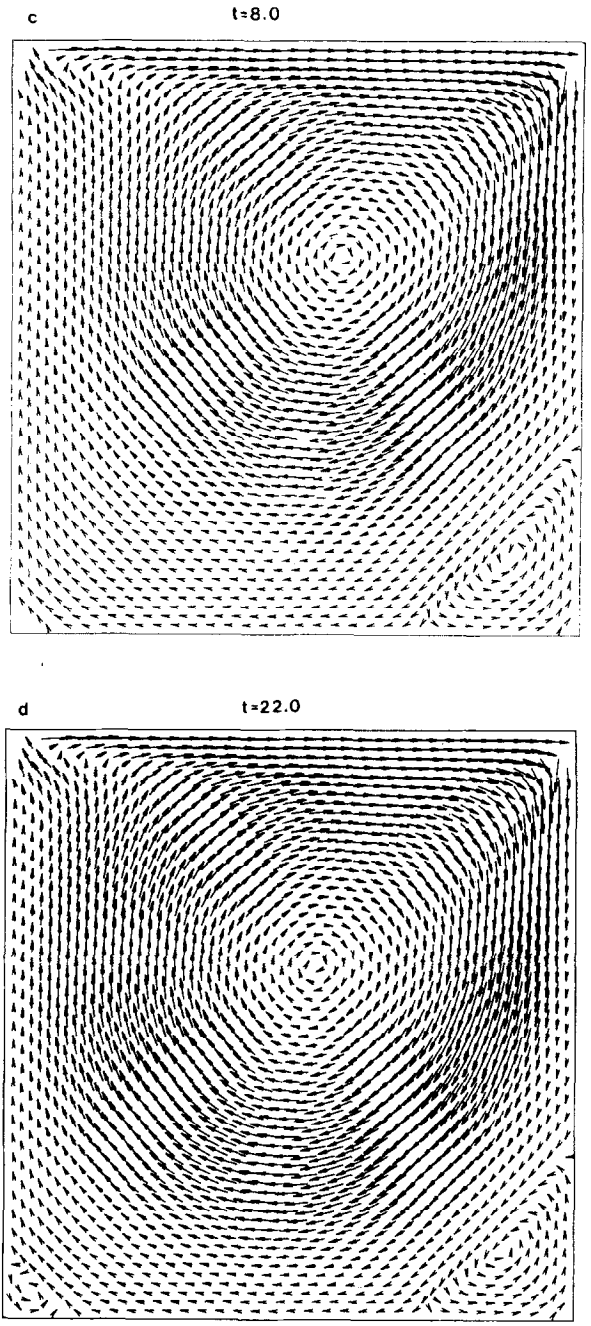

FIGURE 5 (*continued*)

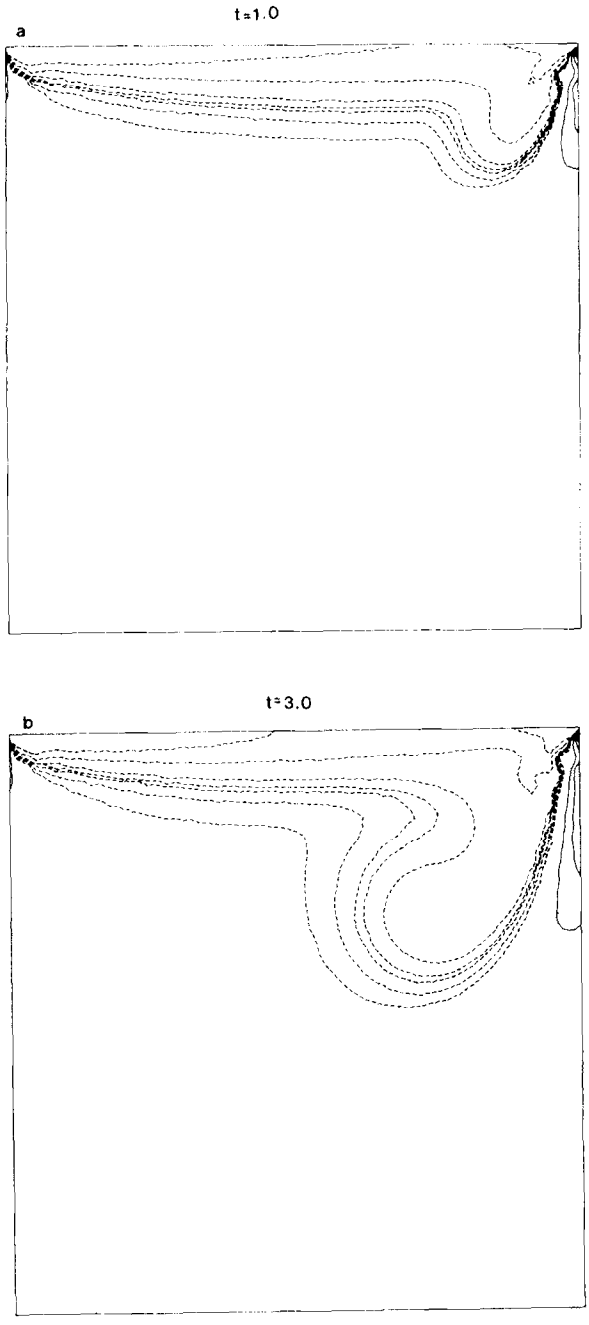

FIG. 6. Evolution of vorticity contours in a square cavity (Re = 400).

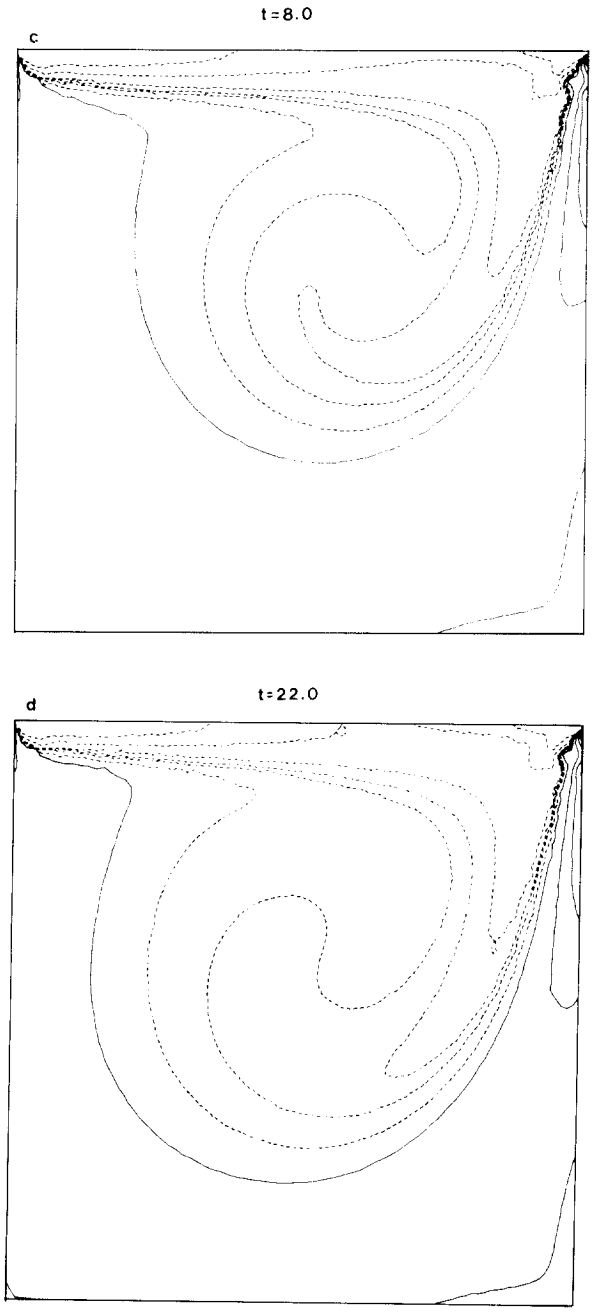

FIGURE 6 *(continued)*

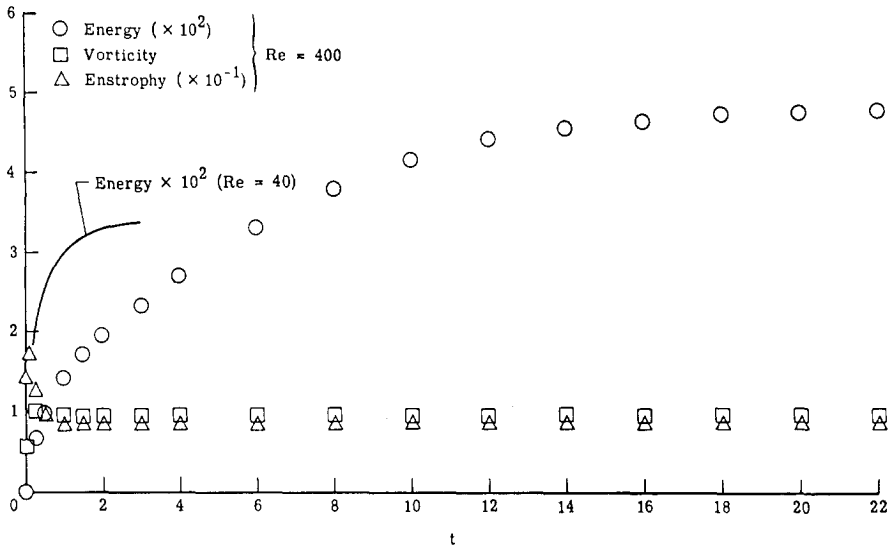

FIG. 7. Evolution of integral flow properties for a square cavity.

the vorticity or enstrophy norms occurs. In contrast, the kinetic energy gradually approaches an asymptotic steady-state value ($t \simeq 22$).

Physical arguments indicate that the time required to reach a steady state is proportional to the Reynolds number. For $\mathrm{Re} = 40$ an experiment verified that the steady state was reached at time $t = 2.2$, i.e., a factor of 10 smaller than the time $t = 22$ associated with $\mathrm{Re} = 400$. This observation also highlights the cost of accurately following the evolution of a cavity flow for large values of Re; the spin-up of the central vortex in a cavity is an inherently slow dynamical process at high Re.

Similar features of the flow associated with a cavity of twice the length are illustrated for $\mathrm{Re} = 400$ in Figs. 8 and 9. At steady state ($t = 16$) two vortices of opposite sign are evident, the stronger being downstream of the weaker.

Schreiber and Keller [9] have recently carried out very extensive calculations of the steady-state flow in a driven cavity, using up to 180×180 cells. In Fig. 10 we show some comparisons of our final steady state results with their work at $\mathrm{Re} = 1000$. We show in Fig. 10a, the variation of the x component of velocity u with y, the distance from the bottom of the cavity at various x positions. The solid lines are the results of Schreiber and Keller obtained with a 140×140 grid and the symbols are our results with a 32×32 grid. In Fig. 10b we show the corresponding results for the variation of the y component of velocity, v, with x. Our results are in fairly good agreement with those of Schreiber and Keller.

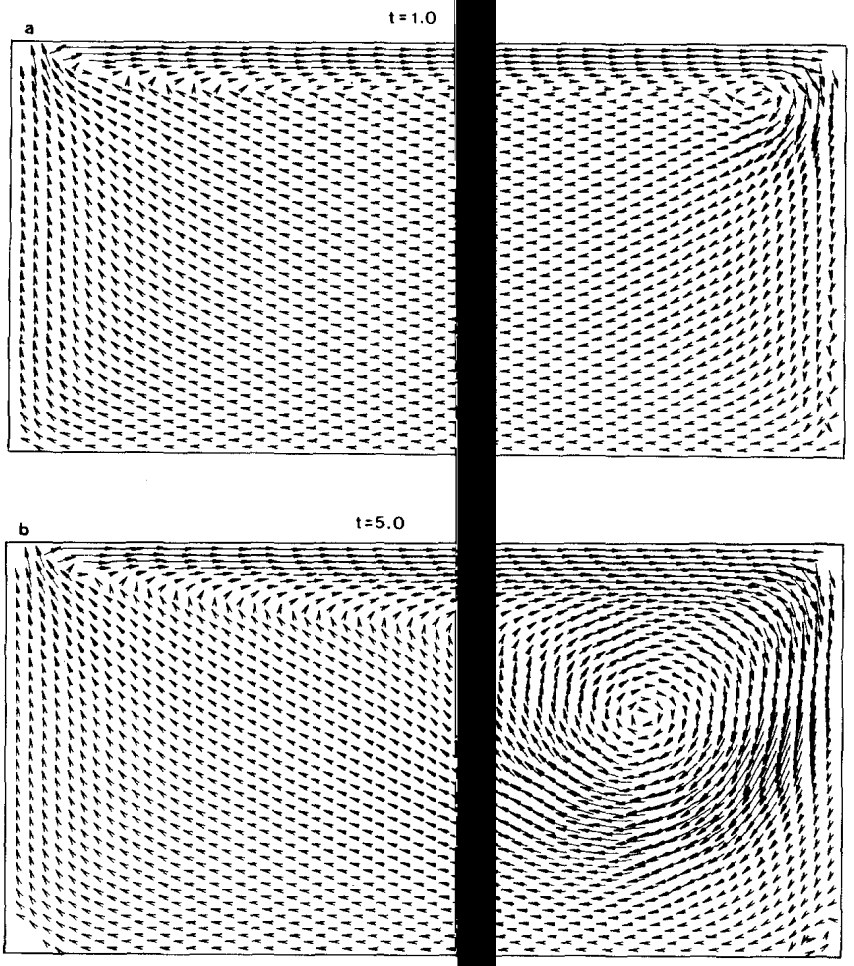

FIG. 8. Evolution of velocity field to steady s in a rectangular cavity (Re = 400).

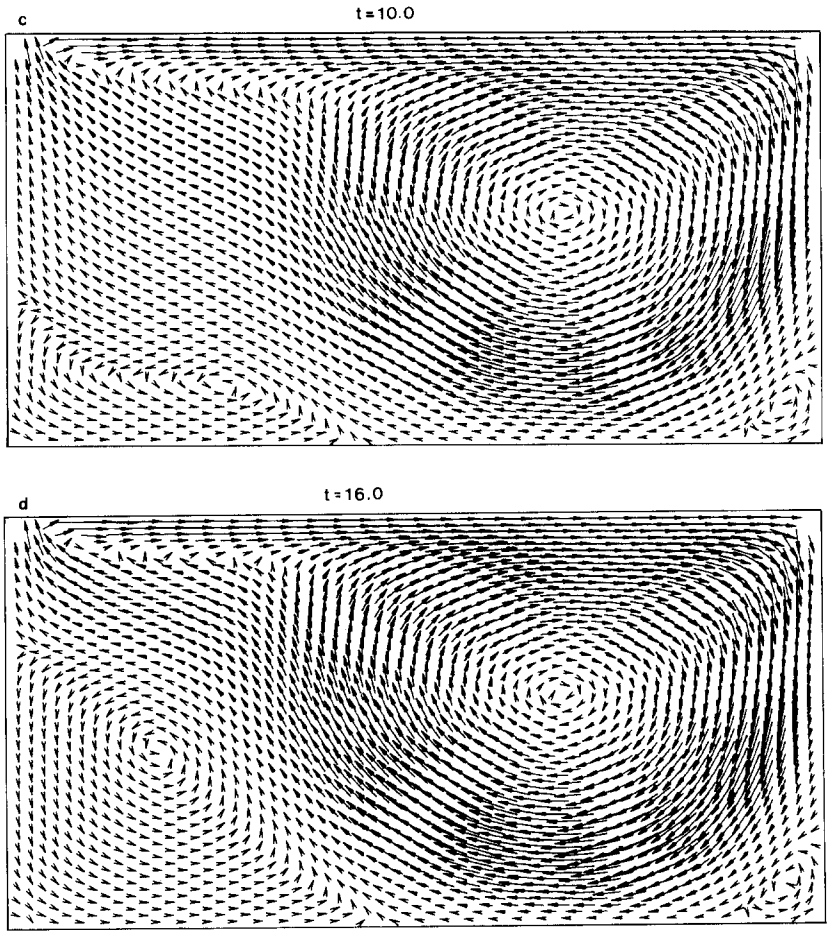

FIGURE 8 (*continued*)

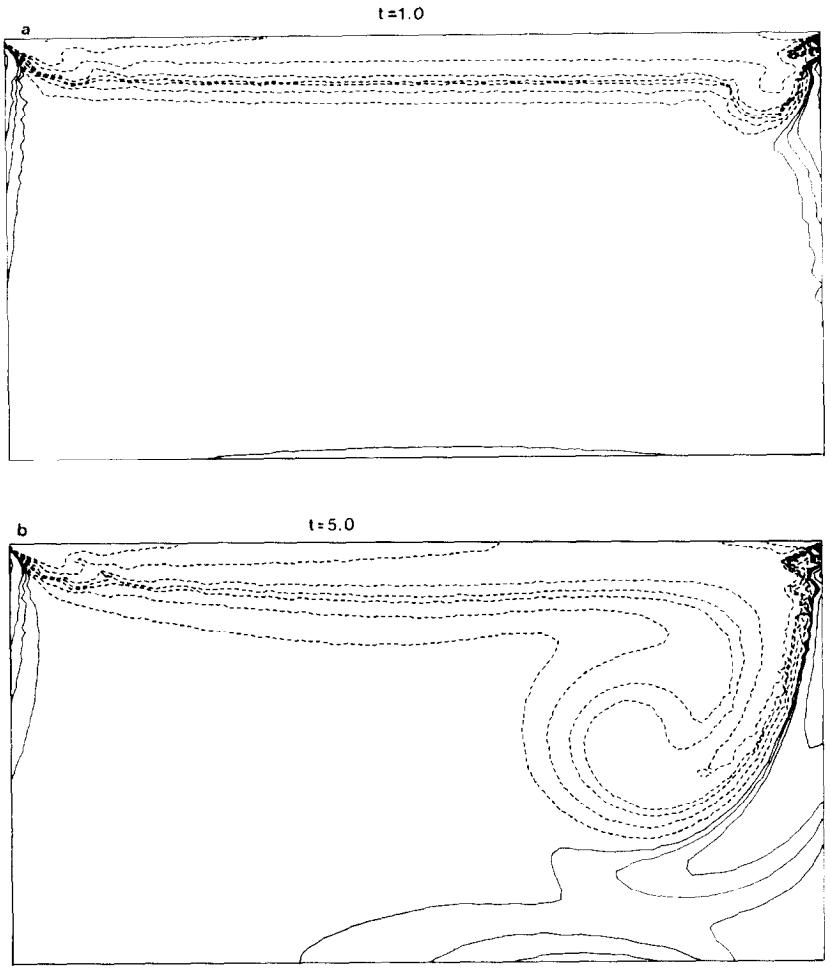

FIG. 9. Evolution of vorticity contours in a rectangular cavity (Re = 400).

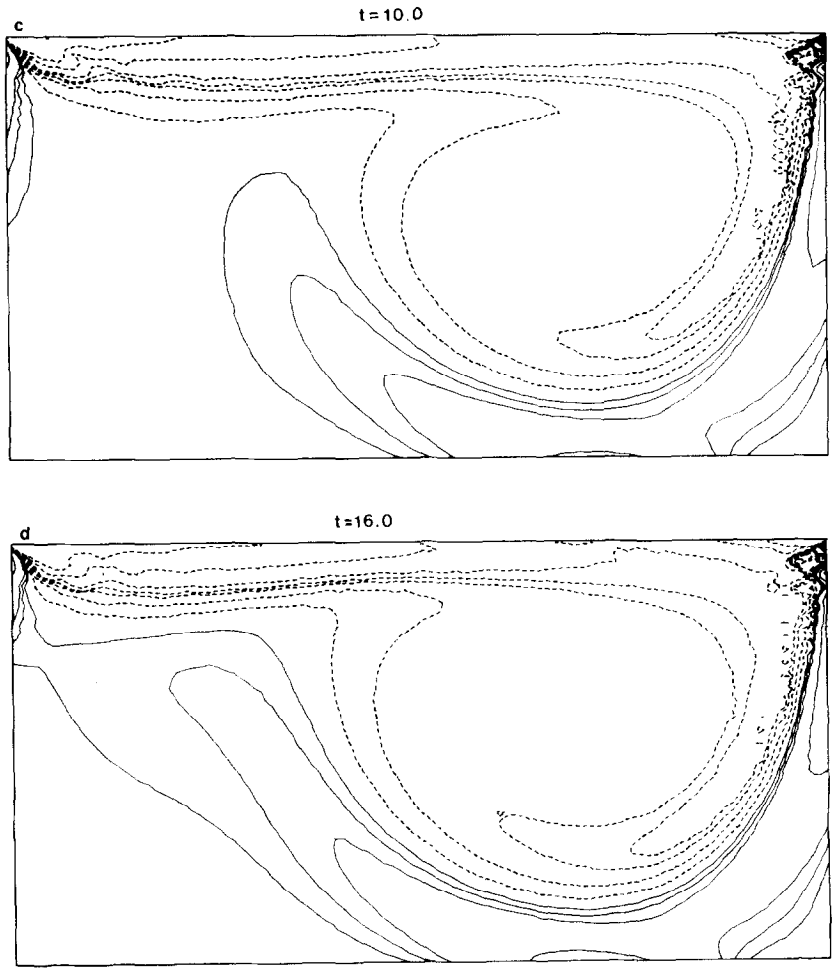

FIGURE 9 (*continued*)

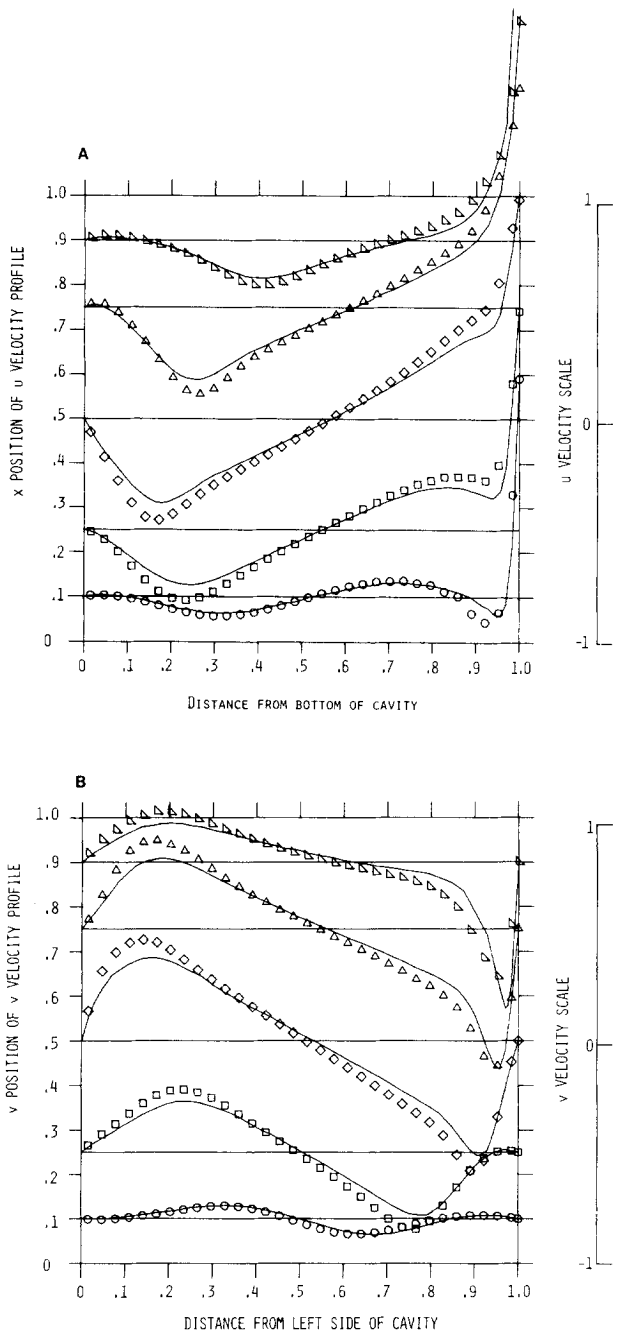

FIG. 10. Comparison of the results of this study with those of Schreiber and Keller. In both of these figures, the solid lines are the results of the calculations of Schreiber and Keller using a mesh 140 × 140 cells, while the symbols are the results of our calculations using 32 × 32 cells.

CONCLUSIONS

Compact difference schemes (2.1) and (2.3) provide a second-order accurate method for solving (1.1) in terms of the velocity and vorticity variables. Numerical experiments with a stagnation flow indicate that the bounary layer may be resolved with as few as two computational cells in order to provide useful engineering accuracy (10%).

The SOR type of iteration scheme employed here to solve velocity equations (2.1) as well as the Δt limitation arising from the ADI algorithm, however, are too inefficient to provide the basis for a generally useful method to obtain steady state solutions. A more efficient approach is now under study and will be reported on in another paper. This development should also permit the direct treatment of steady-state problems related to (1.1).

REFERENCES

1. G. K. BATCHELOR, "An Introduction to Fluid Dynamics" Cambridge Univ. Press, London/New York, 1967.
2. A. S. BENJAMIN AND V. E. DENNY, *J. Comput. Phys.* **33** (1979), 340.
3. L. F. DONOVAN, *AIAA J.* **8** (3) (1970), 524.
4. H. F. FASEL, "Numerical Solution of the Complete Navier–Stokes Equations for the Simulation of Unsteady Flows," Lecture Notes in Mathematics, No. 771, Springer-Verlag, New York/Berlin, 1980.
5. S. KACZMARZ, *Bull. Acad. Pol. Sci. Lett., A* (1937), 355.
6. R. PHILLIPS AND M. E. ROSE, *SIAM J. Numer. Anal.* **19** (4) (1982), 698.
7. P. A. ROACHE, "Recent Developments and Problem Areas in Computational Fluid Dynamics," Lecture Notes in Mathematics, No. 461, Springer-Verlag, New York/Berlin, 1975.
8. M. E. ROSE, *SIAM J. Numer. Anal.* **18** (2) (1981), 372.
9. R. SCHREIBER AND H. B. KELLER, "Driven Cavity Flows by Efficient Numerical Techniques," to appear.
10. K. TANABE, *Numer. Math.* **17** (1971), 203.
11. S. G. RUBIN (Ed.) "Numerical Studies of Incompressible Viscous Flow in a driven Cavity," NASA SP-378, 1975.